Study on the Benefits of Integrated Battery and Cabin Thermal Management in Cold Weather Conditions

Mohammad R. Hajidavalloo, Jun Chen, *Senior Member, IEEE*, Quihao Hu,
and Zhaojian Li, *Senior Member, IEEE*

Abstract— To expand the global adoption of electric vehicles (EVs), improving their driving range is of utmost importance. One of the major obstacles along the way is the degraded EV performance in extremely cold or hot environments, where significant amount of energy is used for cabin and battery temperature regulation while the battery's power and energy capacity are also impeded. To mitigate this issue, we present an integrated cabin and battery thermal management system to simultaneously optimize battery and cabin temperatures in real time. A new nonlinear model predictive control (NMPC)-based thermal management strategy is developed to simultaneously achieve cabin temperature regulation and driving range maximization. The benefits of the proposed integrated thermal management (ITM) of battery and cabin are investigated for cold-temperature driving in various scenarios. Simulation results identify several important factors that affect the EV driving range in cold weather, and we show that up to 7-13% range improvement, relative to the case where only cabin heating is considered, can be achieved using the proposed NMPC-based ITM strategy.

I. INTRODUCTION

The future of transportation will involve a significant proportion of electric vehicles (EVs) on the road, due to the financial effect of high oil prices, environmental impact of fossil fuels such as greenhouse gas emissions, growing interest of public in green and renewable technologies, and regulation and policies for upcoming fuel economy standards [1]. However, there are still daunting barriers to realize EV's wider adoption, including higher marginal price of EVs relative to conventional vehicles, limited battery life span, high cost for battery replacement, limited driving range, and lower performance in cold or hot environments, to name a few [1]. In this paper, we study the impact of cold ambient temperature on EV performance and its mitigation strategies. EVs are affected by cold climates in three major ways. First, a considerable portion of battery energy is consumed for regulating the temperatures of the cabin and the battery. Second, cold weather itself leads to battery performance degradation in terms of lower available energy and power capacity as well as the reduction of battery life. Generally, the poor performance of lithium-ion batteries in cold weather results

from the significant increase of battery internal resistance, which leads to a strong opposing force on a running battery [2]. Third, the driving range of an EV in cold weather conditions is also negatively influenced by the restricted regenerative charging, lower terminal voltage, and reduced capacity, among others. To this end, a battery hardware-in-the-loop study conducted at Argonne National Laboratory indicates that for a plug-in-hybrid EV operating at $-7\ ^oC$, the all-electric-range is reduced by 13% as compared to driving with $0\ ^oC$ ambient temperature, where nearly 34% and 12% of this range reduction are due to the restricted regenerative power and increased thermal resistance, respectively [3]. More extreme conditions and the addition of cabin temperature regulation pose several more challenges on the thermal management of the battery and the cabin in cold climates.

In the literature, the thermal management of battery and/or cabin, for heating or cooling purposes, has been addressed from the control engineering perspective using methods such as nonlinear model predictive control (NMPC) [4]–[8], fuzzy-logic control [9], and dynamic programming (DP) [10], [11]. However, most of the works are focused on cooling controls. For example, [10] proposes an iterative DP-based battery thermal management strategy for connected and automated hybrid EVs. Reference [4], [8], [12] are based on (N)MPC, which aim at minimizing the energy consumption of the thermal management system while satisfying various constraints. In [6], [7], vehicle connectivity is assumed and multi-layer MPC is developed to improve the battery energy efficiency.

Different from the aforementioned works, the focus of this paper is on heating regulation in cold climates, with a specific focus on the tradeoff between driving range and cabin heating requirement. In this context, several efforts have been made to address the battery and cabin thermal management heating issue [5], [13], [14]. Authors in [5] studied the battery thermal management of intelligent-connected EVs at low temperature based on NMPC, where electric heater is used for battery heating and heat pump (HP) is used for the air conditioning system. The results in [5] show that with the developed strategy, the heating duration and energy usage can be decreased. NMPC is also used for the control of cabin temperature and air quality in EVs equipped with HP in cold weathers [13]. Rule-based control of battery external heating for EVs during driving at low temperatures is also studied in [14], where the driving range of EVs is compared with the case where maximum heating power is used as well as with

Mohammad Hajidavalloo, and Zhaojian Li are with the Department of Mechanical Engineering, Michigan State University, East Lansing, MI 48824, USA. Email: {hajidava, lizhaoj1}@msu.edu.

Jun Chen is with the Department of Electrical and Computer Engineering, Oakland University, Rochester, MI 48309, USA. Email: junchen@oakland.edu.

Quihao Hu is with the Department of Naval Architecture & Marine Engineering, University of Michigan, Ann Arbor, MI 48109, USA. Email: qhhu@umich.edu.

the case when battery is not heated. Promising improvements are reported in [14].

Despite the considerable progresses made in the research workes described above, the integrated cabin and battery thermal management for extreme cold condition has not been well studied in the literature. Furthermore, there is a lack of specific assessment of the trade-off between driving range and cabin heating performance, particularly at subzero temperatures. Even though there are a few prior works that have similar scope [3], [14], [15], the model and the made assumptions in these works do not accurately reflect battery performance in low temperatures. For example, in [14], the regenerative power loss is not taken into account, which in fact is one of the major energy loss sources in below-freezing conditions [3], [15].

In this paper, we present an integrated thermal management (ITM) of battery and cabin in cold weather conditions using NMPC, with the focus on its effect on the driving range of EVs. Our findings show that there exists an important compromise between battery performance improvement (due to the battery temperature rise) and the power consumption of the thermal management system. In addition, our simulation results also show that the benefits of EV range improvement due to battery heating depend on different parameters and conditions, such as battery characteristics (e.g., open circuit voltage and internal resistance), ambient temperature, driving cycle profile and behavior, control strategies, driving time, initial SOC, etc. Our contributions are summarized as follows. First, a new NMPC-based ITM strategy for battery and cabin heating is developed to simultaneously optimize EV driving range and cabin comfort. Second, for the proposed ITM system, high-fidelity modeling for each component is developed with relevant parameters listed as a reference for future studies. Third, the important factors that heavily impact the energy loss of the battery in cold weathers are identified through extensive simulations. To the best of the authors' knowledge, this is the first study that focuses on a comprehensive investigation of the impacting factors on the EV driving range in cold weather.

The rest of the paper is structured as follows. In Section II, the proposed ITM system for battery and cabin heating and its modeling are introduced. The NMPC formulation of the ITM problem is presented in Section III, whereas in Section IV simulation results are presented with discussions. Section V concludes the paper.

II. DESIGN & MODELING

We begin this section with a description of the operation conditions considered in the proposed ITM, followed by detailed model derivations of each thermal component. Specifically, Fig. 1 shows the coolant cycle of the integrated battery and cabin thermal management (heating) system under consideration. Firstly, the coolant with flow rate $\dot{m}$ and temperature T_4 is heated to temperature T_1 by a heat pump (HP). The heated coolant then arrives at the 3-way valve, where the coolant flow rate for the cabin and battery branch is regulated by the controller. The coolant flow for the
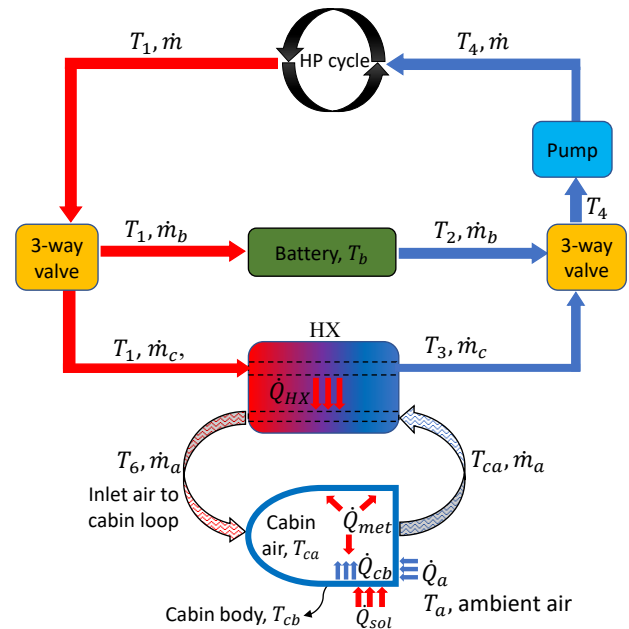

Fig. 1: Schematics of the integrated battery and cabin thermal management (heating) system.

cabin heating passes the heat exchanger (HX) and indirectly heats the inlet air to the cabin and becomes cooled, the rate of which is denoted by $\dot{m}_c$. The inlet air to the cabin heats the cabin air and then goes back to the HX to complete the cycle. On the battery side, the battery is heated by the coolant flowing in the battery branch, denoted by $\dot{m}_b$. Then, the coolant flow for cabin and battery are mixed to reach temperature T_4 and pumped towards the HP, which completes the coolant cycle. In the following, we elaborate more on each component of the proposed integrated battery and cabin thermal management system.

A. Heat pump model

As shown in Fig. 1, the coolant with low temperature T_4 is heated by a separate Heat Pump (HP), the heat rate of which is denoted by $\dot{Q}_{HP}$, and it reaches a higher temperature T_1 that is necessary for further circulation of the coolant to heat the cabin and the battery as will be shown in subsequent texts. The governing equations for this heat exchange are:

$$C_1 \dot{T}_1 = \dot{Q}_{HP} + \dot{m} c_c (T_4 - T_1), \tag{1a}$$

$$\dot{m} = \dot{m}_b + \dot{m}_c, \tag{1b}$$

where $C_1 = m_{clnt} c_c$ is the thermal inertia of the heated coolant, m_{clnt} is the total mass of the coolant in the cycle, c_c is the specific heat capacity of the coolant, and $\dot{m}$ is the total coolant flow rate. The coolant liquid is G-48 ethylene-glycol which is a common choice for vehicles thermal loop. The use of HP instead of PTC heater has advantages such as achieving coefficient of performance (COP) higher than one, thus improving the mileage of EVs. Note that HP has already been deployed by EV makers such as Tesla (e.g., Tesla Model Y) and Nissan (e.g., Nissan Leaf) [16],

[17]. More details on HP components and its modeling are omitted here due to space limit. The experimental data studied in [18] can be utilized to calculate the HP's electrical power consumption. In [18] the performance of an EV's HP is evaluated experimentally in cold climate conditions and in this paper, the heating capacity and the COP of the HP follow from their experimental studies. According to the findings of [18], at a fixed ambient temperature, fixed indoor air recirculated percentage, fixed outdoor air velocity (i.e. ram-air) and fixed inlet air flow rate, COP and heat capacity change linearly w.r.t compressor speed so one can easily interpolate the performance of the HP based on the experimental data. Interested readers are referred to [18] for more details on the experiments resulting in quantifying the HP performance. In this regard, by only considering ambient temperatures and compressor speeds as variables and assuming fixed indoor air recirculated percentage, fixed outdoor air velocity and inlet air flow rate, the heat provided by HP follows from the definition of the COP, i.e.,

$$COP_{HP}(T_{amb}, n_{comp}) = \frac{\dot{Q}_{HP}(T_{amb}, n_{comp})}{P_{elec}}, \quad (2)$$

where COP_{HP} stands for the coefficient of performance of the HP cycle, $\dot{Q}_{HP}$ is the heat capacity, and P_{elec} is the electric power consumption of the HP mostly from compressor. In this regard, we take the compressor speed, n_{comp}, into consideration as another control variable. Once n_{comp} is chosen and T_{amb} is known, the experimental data study in [18] can be used to determine the amount of electricity used by the HP.

B. Cabin heat exchanger (HX) and cabin dynamics

Modeling a car cabin from a thermal perspective is challenging, particularly when it includes an HVAC system, since there are several components and a lot of influences should be considered [13]. Moreover, for real-time implementation of NMPC, a non-complex model is needed for tractable real-time computations. This model should also be detailed enough to accurately predict the thermal behaviors of the cabin. In this regard, we follow the developments in [13], [19] for modeling the inlet air to cabin heat exchange as well as the cabin air dynamics. The models proposed therein are straightforward with accurate representations of real dynamics, and the parameters are determined or estimated based on actual experimental data. As previously mentioned, the coolant flow rate for the cabin branch, $\dot{m}_c$, is determined by the model predictive controller. This flow with high temperature T_1 passes through a HX that heats the inlet air to cabin and exits that with low temperature T_3. The heated inlet air with high temperature T_6 enters the cabin with flow rate $\dot{m}_a$, heats the cabin air with temperature T_{ca} and reaches the cabin temperature, and then exits the cabin. Accordingly, the heat exchange between coolant and the cabin inlet air loop can be modeled by the following two equations:

$$C_3\dot{T}_3 = \dot{m}_c c_c(T_1 - T_3) - G_{HX}(T_3 - T_6), \quad (3a)$$
$$C_6\dot{T}_6 = c_a\dot{m}_a(T_{ca} - T_6) + G_{HX}(T_3 - T_6), \quad (3b)$$

where (3a) characterizes the heat exchange for the cabin branch coolant mass in the HX and (3b) formulates the heat exchange for the inlet air to cabin mass. In these two equations, $C_3 = m_{clnt,c}c_c$ is the thermal inertia of the coolant in the cabin branch, $m_{clnt,c}$ stands for the cabin branch coolant mass, $C_6 = m_a c_a$ is the thermal inertia of the inlet air to cabin, m_a is the inlet air mass, c_a is the specific heat capacity of air, and G_{HX} is the heat transfer coefficient between the inlet air and the coolant.

For modeling the various elements of cabin components, it should be noted that the cabin air – the most important element for the thermal management task – has interaction with the inlet air to the cabin, the cabin body, cabin shell and interior, the passengers, solar radiation, etc. The inlet air to the cabin serves as the primary heating element of the cabin components. For modeling the cabin dynamics, we consider the following second order model [19], [20] which considers the cabin air and cabin body as state variables:

$$C_{ca}\dot{T}_{ca} = \dot{m}_a c_a(T_6 - T_{ca}) + \dot{Q}_{met} + \alpha_{cb}A_{cb}(T_{cb} - T_{ca}),$$
$$(4a)$$
$$C_{cb}\dot{T}_{cb} = -\alpha_{cb}A_{cb}(T_{cb} - T_{ca}) + \dot{Q}_{sol} + \alpha_{ab}A_{ab}(T_a - T_{cb}),$$
$$(4b)$$

where Equation 4a represents the cabin air temperature dynamics, and Equation 4b represents the vehicle body temperature dynamics. Equation 4a summarizes the most important factors that affect the cabin air temperature, including the inlet air to cabin (the first term on the right), $\dot{Q}_{met}$ that accounts for the metabolic heat from the passengers, and the heat exchange with other components such as cabin shell, window, wall as represented by the last term and denoted by heat exchange with cabin body. In Equation 4a, α_{cb} is the lumped heat transfer coefficient per unit area, A_{cb} is the heat transfer surface area between the cabin air and cabin body, T_{cb} is the cabin body temperature, and lastly $C_{ca} = m_{ca}c_a$ is the cabin air thermal inertia with m_{ca} is the cabin air mass. In Equation 4b, the first term on the right side accounts for the heat transfer from cabin air to the cabin body; the second term accounts for the heat absorbed by the sun; and the last term accounts for the heat transfer between the ambient air and the cabin body. Here $C_{cb} = m_{cb}c_{cb}$ is the cabin body thermal inertia with m_{cb} being the cabin body mass and c_{cb} being the specific heat capacity of the cabin body.

C. Pump model

As shown in Fig. 1, the pump is placed after the 3-way-valve that mixes the coolant flow from battery and cabin before reaching HP. The mixing temperatures of the fluid can be established as

$$T_4 = \frac{1}{\dot{m}}(\dot{m}_b T_2 + \dot{m}_c T_3). \quad (5)$$

The pump task is to maintain the desired flow rate by performing mechanical work to the coolant. The power consumption of the pump is represented by:

$$P_{pump} = \frac{P_{pump,m}}{\eta_m} = \frac{1}{\eta_m} \cdot \frac{\Delta p_{pump}\dot{m}}{\rho_c}, \quad (6)$$
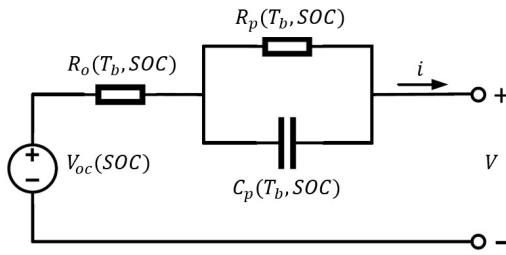
Fig. 2: RC

where $P_{pump,m}$ is the mechanical power, η_m is the power conversion rate of the pump, ρ_c is the coolant density, Δp_{pump} is the pressure drop of the pump, which is related to the mass flow rate of the coolant and takes the following form [5]:

$$\Delta p_{pump} = 0.927\dot{m}^2 + 0.586\dot{m} - 0.143. \tag{7}$$

D. Electrothermal battery model and battery pack

The battery cell used to construct the battery pack is modeled using the popular Equivalent Circuit Model (ECM) [2], [21], [22]. As shown in Fig. 2, V_{oc} denotes the open-circuit voltage of the cell; R_o is the ohmic resistance; R_p and C_p are the polarization resistance and capacitance respectively. Furthermore, i is the current with positive value for discharge and V denotes the output voltage (or terminal voltage) of the cell. V_o is the voltage drop on R_o and V_p is the polarization voltage on R_p. The dynamics of the $R - C$ pair can be represented by:

$$\dot{V}_p = -\frac{V_p}{R_pC_p} + \frac{i}{C_p}, \tag{8}$$

and the terminal voltage of the battery is

$$V_{oc} - iR_o - V_p - V = 0. \tag{9}$$

In order to maintain the model's accuracy, it is crucial to take into account the variation of the open circuit voltage V_{oc} with respect to state-of-charge (SOC). Similarly, the ohmic resistance, polarization resistance and capacitance's variation with both battery temperature and SOC, is considered as discussed in [2]. The battery cell SOC dynamics is specified by

$$\dot{SOC}_{cell,i} = -\frac{i}{3600 \times C_{cell}}, \tag{10}$$

where C_{cell} is the cell capacity in Ah.

We assume that the battery pack is grouped by identical cells with similar initial SOC in our simulations, through S in series and P in parallel. Since the dynamic response of the RC circuit has almost reached steady state after a brief period of time, it can be assumed that the current flowing through the polarization resistor is equal to the overall current [14]. Hence one can write

$$R_{pack} = S(R_o + R_p), \tag{11a}$$
$$i_{pack} = Pi, \tag{11b}$$
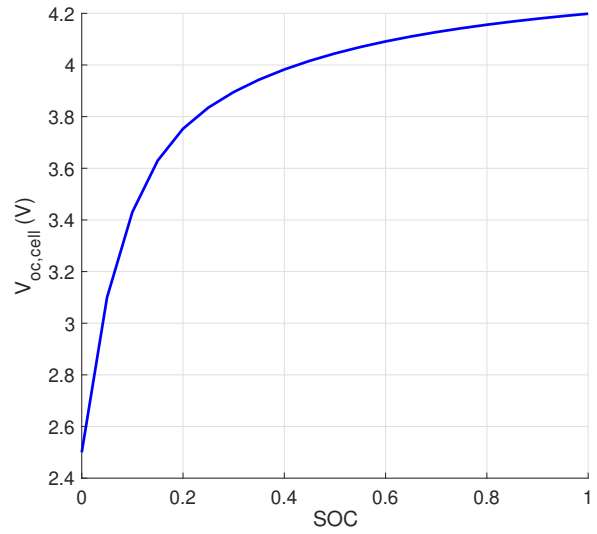$$V_{oc,pack} = SV_{oc}, \tag{11c}$$

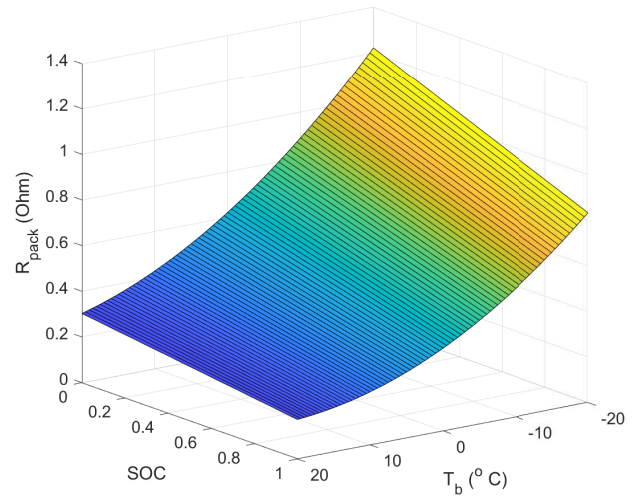
Fig. 3: Open circuit voltage values with respect to SOC.

Fig. 4: Internal resistance of the battery pack with respect to SOC and battery temperature.

where R_{pack}, i_{pack} and $V_{oc,pack}$ are the overall ohmic resistance of the battery pack, current of the battery pack and open circuit voltage of the battery pack, respectively. The internal resistance of the battery pack and the open circuit voltage of the battery cell used in our simulations correspond to the behaviors depicted in Figs. 3 and 4. Furthermore, the battery pack SOC is the averaged SOC across the battery cells, which equals to, with the identical cell assumption, each battery cell's SOC:

$$SOC = \frac{SOC_{cell,1} + SOC_{cell,2}, + \cdots + SOC_{cell,NP}}{NP}$$
$$= SOC_{cell,i} = -\frac{i_{pack}}{3600 \times C_{pack}}. \tag{12}$$

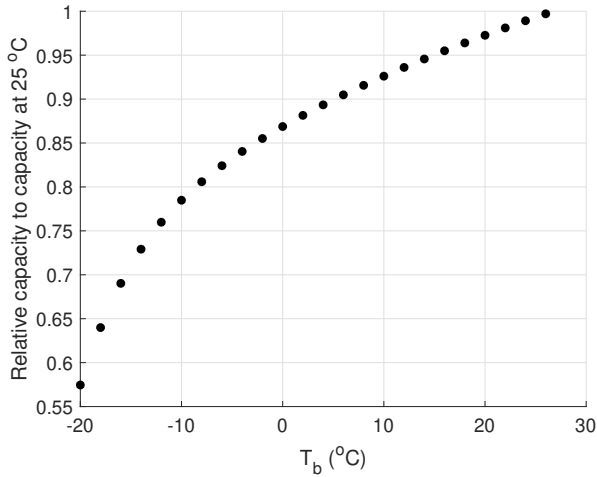According to [1], [3], [15], the battery capacity is also

Fig. 5: Relative capacity with respect to temperature.

dependent on the battery temperature, and we use the data from [1] to quantify the available percentage of battery capacity relative to the capacity at 25^oC versus battery temperature. This is shown in Fig. 5.

For modeling the thermal behavior of the battery, the battery pack is considered as a lumped mass with specific heat capacity c_b, mass of m_b and temperature T_b. The coolant flow rate for the battery, $\dot{m}_b$, is determined via the model predictive controller, and the battery is heated by the coolant which enters the battery from one side with high temperature T_1 (see Fig. 1), circulates around the battery and exits from the other side of the battery with cooled temperature T_2. Based on this, one can write the differential equation for the battery temperature as:

$$C_b\dot{T}_b = R_{pack}i_{pack}^2 + \dot{m}_b c_c(T_1 - T_2) - h_a(T_a - T_b). \quad (13)$$

Here $C_b = c_b m_b$ is the thermal inertia of the battery, and the first term on the right considers the internal heat generation of the battery. The second term in (13) accounts for the heat from the coolant to the battery, the third term is the heat transfer rate between battery and the ambient air where T_a is the ambient air and h_a is the heat transfer coefficient between the ambient air and the battery pack. Accordingly, we write the energy balance equation for the coolant, which expresses the heat exchange between coolant and battery as:

$$C_2\dot{T}_2 = \dot{m}_b c_c(T_1 - T_2) - h_b A_b(T_2 - T_b). \quad (14)$$

In this equation, $C_2 = m_{clnt,b}c_c$ with $m_{clnt,b}$ being the coolant mass that heats the battery. The first term on the right hand side characterizes the energy balance of the coolant and the second term accounts for the heat loss of the coolant when it does the heat transfer with the battery with the heat transfer coefficient per unit area h_b and the heat transfer surface area A_b .

E. Battery power demand

The traction power demand for vehicle's movement can be written as [7]:

$$P_{trac} = V_{veh}\left(F_r + F_a + M\dot{V}_{veh}\right), \quad (15)$$

where $V_{veh}, \dot{V}_{veh}, M$, are vehicle speed, vehicle acceleration, and vehicle mass, respectively. The following formulas are used to compute the rolling (F_r) and aerodynamic (F_d) resistance forces:

$$F_r = C_r Mg, \quad (16a)$$
$$F_a = 0.5\rho_a A_f C_d V_{veh}^2, \quad (16b)$$

where C_r and C_d are, respectively, the rolling resistance and aerodynamic drag coefficients, A_f is the vehicle frontal area, and ρ_a is the air density. Combining the HP consumed power and electric pump power (6), the total thermal power required is

$$P_{TM} = P_{elec} + P_{pump}. \quad (17)$$

Therefore, the total battery power can be denoted as

$$P_{tot} = P_{TM} + P_{trac}, \quad (18)$$

and the battery pack current can be subsequently calculated by

$$i_{pack} = \frac{V_{oc,pack} - \sqrt{V_{oc,pack}^2 - 4R_{pack}P_{tot}}}{2R_{pack}}. \quad (19)$$

Remark II.1. *Maximizing the driving range is equivalent to minimizing the current i_{pack} drawn from the battery. According to (12), (18) and (19), short-term battery current minimization can be achieved by the following: 1) enabling battery charging from regenerative power by increasing battery temperature to charge-permitted value; 2) decreasing R_{pack} by increasing battery temperature to optimal value; 3) increasing battery capacity C_{pack} by increasing battery temperature to optimal value; and 4) decreasing P_{tot} by decreasing P_{TM}. Therefore, to maximize EV range for a short-term horizon, one can either increase battery temperature to optimal value, and/or decrease the thermal management power P_{TM}.*

III. NONLINEAR MPC FORMULATION

In this section we introduce the ingredients of the NMPC problem for the proposed ITM of battery and cabin heating. The governing equations of the ITM system are described in the previous section. Herein, we directly denote the continuous-time nonlinear dynamics of the ITM system as follows

$$\dot{x} = f_c(x, u, p), \quad (20)$$

where the state vector, the control inputs, and the parameter are defined as follows

$$x = [SOC, T_b, T_3, T_1, T_2, T_6, T_{ca}, T_{cb}]^T,$$
$$u = [\dot{m}_c, \dot{m}_b, n_{comp}]^T, \qquad p = P_{trac}, \quad (21)$$

and the nonlinear continuous function $f_c(.)$ is the equations defined as (1)-(19). The main goal for using NMPC to regulate the temperatures of the passenger cabin and battery is to simultaneously improve the EV range and satisfy the cabin heating requirements, by indirectly controlling the energy consumption of the integrated thermal management system (we will elaborate more on our usage of "indirect control" after defining the stage cost). In this regard we define the stage cost of the NMPC as follows:

$$l(x, u) = \alpha(T_{ca} - T_{ca,sp})^2 + (T_b - T_{b,sp})^2, \quad (22)$$

where the first and second terms penalize the deviation of the cabin and battery temperatures from their set points, respectively; and α is the corresponding weight to express the trade-off between each cost terms. Consequently, the finite receding-horizon optimal control problem at each time step is defined as follows:

$$V_N^0(x_0) = \min_{u(0),...,u(N-1)} V(x_0, u) = \sum_{k=0}^{N-1} l(x(k), u(k))$$
$$\text{s.t. } x(0) = x_0, x(k+1) = f_d(x(k), u(k))$$
$$x_{min} \le x(k) \le x_{max}, \ k = 0, \ldots, N$$
$$g_{min} \le g(u(k)) \le g_{max}, \ k = 0, \ldots, N-1. \quad (23)$$

In the above constrained optimal control problem, N is the prediction horizon, x_0 is the initial state, $f_d(.)$ is the discretized version of $f_c(.)$ with proper sampling time T_s, x_{min} and x_{max} are the lower and upper bound values of the states and g_{min} and g_{max} are the lower and upper bound values of the constraint function for control inputs. The values for the lower and upper bounds of state variables and the constraint function for control inputs will be specified in the next section.

Remark III.1. *We refer to the stage cost (22) as "indirect" approach, since it includes battery temperature tracking as opposed to battery current minimization. A more direct approach to formulate NMPC (23) is then to include a power consumption term (e.g., P_{TM}^2, similar to work [5]) or a current term i_{pack} in the cost function, as this directly relates to EV driving range and would lead to battery temperature optimization. See Remark II.1. However, through simulation it was discovered that for such direct NMPC formulation, the positive impact of increasing battery temperature cannot be predicted even with a long prediction horizon of 300 seconds. Instead, the controller would completely shut off battery heating to minimize the short-term battery current. Further investigation on this issue and devising novel control strategies to enable a long horizon forecast is the subject of our future work.*

During the implementation of the NMPC, the following considerations are incorporated to preserve battery safety and longevity. First, the lithium-ion cell's terminal voltage must be kept within a particular range during charge and discharge, denoted by the symbols $V_{cut,ch}$ and $V_{cut,disch}$, respectively, which can be temperature-dependent as well.
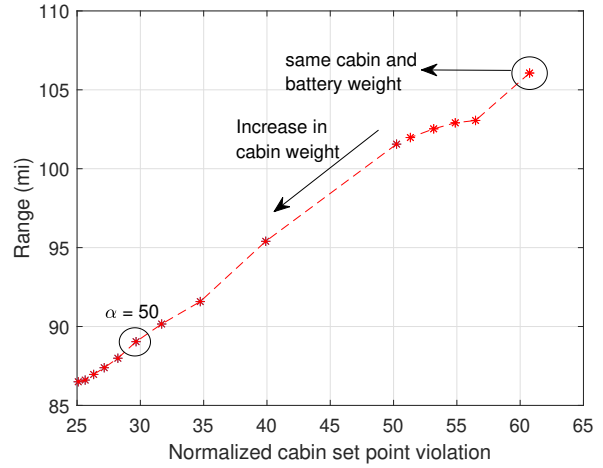

Fig. 6: Different trade-off between range and cabin set point violation by varying α in the stage cost (22).

Second, during the EV operation, charging the battery by the regenerative power is forbidden below a specific battery temperature (usually $0^o\,C$) to prevent battery degradation and decrease plating. Lastly, when allocating battery power among various vehicle components, priority should be given to the traction power demand. In other words, if the above mentioned factors impose limit on the power output of the battery, resulting in a compromise between addressing the thermal management power demand and the traction power demand, then a separate controller overrides the NMPC control strategy and prioritizes the traction power, and the remaining power is assigned to the thermal management.

IV. SIMULATION RESULTS

In this section, the simulation results of the proposed ITM system for battery and cabin heating are presented. We next introduce the detailed simulation setup. Specifically, the lower and upper bounds of the states in (23) are defined as:

$$x_{min} = [0, T_a, T_a, T_a, T_a, T_a, T_a, T_a]^T,$$
$$x_{max} = [1, 25, 70, 70, 70, 70, 25, 25]^T, \quad (24)$$

where T_a presents the ambient temperature and all the temperatures are in Celsius degrees. The input constraints are defined by $g_{min} \le g(u) = [u(1), u(2), u(3), u(1)+u(2)]^T \le g_{max}$, where g_{min} and g_{max} are defined as:

$$g_{min} = [0, 0, 0, 0]^T, \ g_{max} = [0.2, 0.2, 6000, 0.2]^T, \quad (25)$$

where the mass flow rate unit is kg/s and the compressor speed unit is rpm. A complete list of simulation parameters are shown in Table I. The traction power parameters in Equation 16 are adopted from [6]. In the prediction horizon the values for the traction power (which depends on the future velocity and acceleration profiles and may not be known in advance) is assumed constant and equal to the current time power traction demand.

Three different control strategies are implemented and compared. In the first strategy, we set $\alpha = 1$ in the stage

TABLE I: Simulation parameters

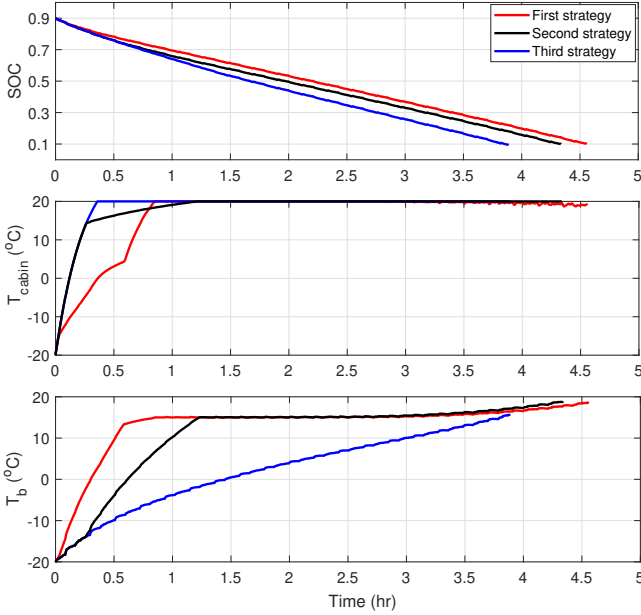| $T_s[s]$	N	$V_{cut,disch}[V]$	$V_{cut,ch}[V]$	$c_c[\frac{J}{kgK}]$	$C_{pack}^{nom}[Ah]$	$A_b[m^2]$	$h_b[\frac{W}{m^2K}]$	$h_a[\frac{W}{K}]$	$m_{clnt}[kg]$
0.5	20	2.5	4.25	2433	185	3	500	15	15
$m_b[kg]$	$c_b[\frac{J}{kgK}]$	η_{pump}	$\rho_c[\frac{kg}{m^3}]$	$m_{clnt,b}[kg]$	$m_{clnt,c}[kg]$	$G_{HX}[\frac{W}{K}]$	$c_a\frac{J}{kgK}$	S,P	$m_a[kg]$
250	1130	0.95	1114	11.75	3.25	400	1008	96,3	0.129
$\dot{m}_a[\frac{kg}{s}]$	$m_{ca}[kg]$	$\dot{Q}_{met}[W]$	$\dot{Q}_{sol}[W]$	$\alpha_{cb}[\frac{W}{m^2K}]$	$\alpha_{ab}[\frac{W}{m^2K}]$	$A_{cb}[m^2]$	$A_{ab}[m^2]$	$m_{cb}[kg]$	$c_{cb}[\frac{J}{kgK}]$
0.125	4.25	400	200	30	500	5	8	50	840

Fig. 7: SOC, cabin temperature and battery temperature v.s. time for HWFET using 3 different control strategies.

Fig. 8: Range and cabin set point violations under various impacting conditions

cost (22), representing a same weight for the cabin and battery set point regulation. The second strategy aims at finding a proper trade-off between the driving range and the normalized cumulative cabin set point violation term defined as $\Sigma_t 10^{-4}(T_{ca,sp}-T_{ca})^2$. In this regard, by varying α in the range of $(1,100]$ and plotting the Pareto optimal points, the α value that offers a good trade-off is found to be $\alpha = 50$ (see Fig. 6). The third strategy is to perform cabin heating only by setting $\alpha = 0$ in the stage cost.

Our simulation results show that there exists an important trade-off between battery performance improvement due to the battery temperature rise and the power consumption of the thermal management system. This compromising issue is of paramount importance and the benefits of EV range saving by battery heating depend on different parameters and conditions such as temperature and SOC-dependent battery's characteristic (e.g., open circuit voltage and internal resistance), ambient temperature, driving cycle profile and behavior, different control strategies, driving time, initial SOC, among others.
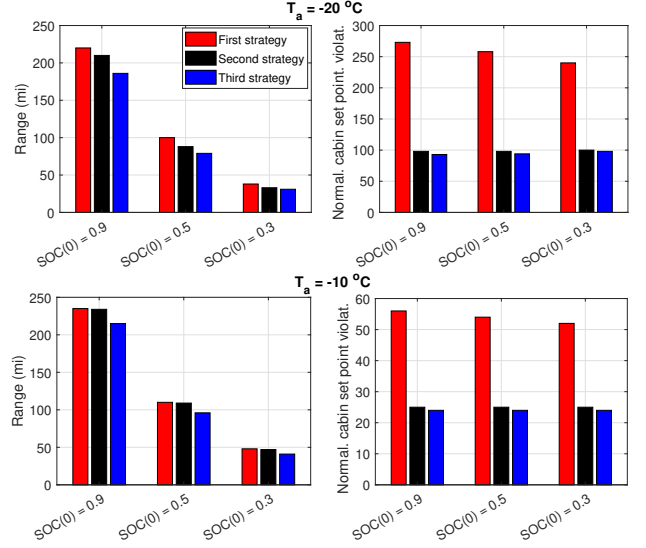
To this end, the first set of results consider the ambient temperature $T_a = -20^oC$ and use repeated HWFET driving cycle as a relatively intensive driving behavior. The state initial condition vector is considered as $x_0 = [0.9, -20, -20, -20, -20, -20, -20, -20]^T$ with a nearly full initial SOC. The simulation is terminated whenever the battery pack SOC drops below 0.1. The battery and cabin set point temperatures are set to 15^oC and 20^oC, respectively. The plot in Fig. 7(a) shows that the first strategy offers the best range with an increase of more than 20 min driving time compared to the other two strategies. However, it can be seen from Fig. 7(b) that the first strategy takes the longest time for cabin to reach the set point among three strategies. In this regard, as we mentioned above, the second strategy was proposed to achieve best trade-off between range improvement and cabin comfort. It is clear that with the second strategy the cabin temperature reaches to its set point sooner. Finally, although the third strategy can regulate the cabin temperature reach to the set point rather quickly, the driving range is substantially less, e.g., by 33 mins compared to the second strategy and 48 mins compared to the first strategy.

In Fig. 8, we repeated the same study by considering

two more initial SOCs, i.e., 0.5, and 0.3 and with another ambient temperature of $T_a = -10^oC$. The results show that in all cases the proposed ITM heating strategy improves the EV range. With $T_a = -20^oC$, and with $SOC(0) = 0.9, 0.5, 0.3$ the range is improved by $12\%, 11\%, 7\%$, respectively, relative to the case with only cabin heating. For $T_a = -10^oC$ these corresponding values are $9\%, 12\%, 13\%$. It is worth noting that higher ambient temperature (i.e., $T_a = -10$) improves the EV range by making the HP more efficient, i.e., it uses less electric power to create the same quantity of heat when the ambient temperature is higher. Also, it makes the battery to reach to the permitted-charge temperature sooner. However $T_a = -10$ reduces the generated self-heat of the battery by decreasing the internal resistance (R_{pack}). Additionally, with lower SOCs, the battery pack can also use more of the regenerative power due to reduced battery voltage w.r.t. higher SOCs. The overall effect of these phenomena will result in a rise in the range improvement percentage by the decrease of the initial SOC, when the ambient temperature is changed from $T_a = -20^oC$ to $T_a = -10^oC$.

V. CONCLUSION

In this paper, we considered the problem of integrated battery and cabin heating for electric vehicles (EV) in cold conditions. A novel NMPC-based integrated thermal management (ITM) strategy for battery and cabin is proposed to simultaneously optimize EV driving range and cabin comfort. High-fidelity models of different components of the ITM system are developed, together with an indirect approach defining the cost function to achieve the optimal energy saving and cabin set point regulation. To analyze the compromise between battery performance improvement and the power consumption of the thermal management system, extensive simulations are performed and our results show that up to 13% driving range improvement can be achieved by the proposed NMPC-based ITM system while the violation of the cabin set point temperature is also minimized. Our results also identified important factors affecting the EV driving range, i.e. temperature and SOC-dependent battery's characteristic (e.g., open circuit voltage and internal resistance), ambient temperature, driving cycle profile and behavior, different control strategies, driving time, initial SOC, etc. Future work will focus on improving the NMPC-based control strategies, e.g. by incorporating practical ways for having longer prediction horizons. Comparison with other benchmark control approaches will also be included in our future work.

REFERENCES

[1] A. A. Pesaran, S. Santhanagopalan, and G.-H. Kim, *Addressing the impact of temperature extremes on large format li-lon batteries for vehicle applications*. National Renewable Energy Laboratory, 2013.

[2] J. Jaguemont, L. Boulon, and Y. Dubé, "Characterization and modeling of a hybrid-electric-vehicle lithium-ion battery pack at low temperatures," *IEEE Transactions on Vehicular Technology*, vol. 65, no. 1, pp. 1–14, 2015.

[3] N. Shidore and T. Bohn, "Evaluation of cold temperature performance of the jcs-vl41m phev battery using battery hil," *Evaluation*, vol. 1, p. 1333, 2008.

[4] Y. Ma, H. Ding, H. Mou, and J. Gao, "Battery thermal management strategy for electric vehicles based on nonlinear model predictive control," *Measurement*, vol. 186, p. 110115, 2021.

[5] Y. Ma, H. Ding, Y. Liu, and J. Gao, "Battery thermal management of intelligent-connected electric vehicles at low temperature based on nmpc," *Energy*, vol. 244, p. 122571, 2022.

[6] M. R. Amini, H. Wang, X. Gong, D. Liao-McPherson, I. Kolmanovsky, and J. Sun, "Cabin and battery thermal management of connected and automated hevs for improved energy efficiency using hierarchical model predictive control," *IEEE Transactions on Control Systems Technology*, vol. 28, no. 5, pp. 1711–1726, 2019.

[7] M. R. Amini, I. Kolmanovsky, and J. Sun, "Hierarchical mpc for robust eco-cooling of connected and automated vehicles and its application to electric vehicle battery thermal management," *IEEE Transactions on Control Systems Technology*, vol. 29, no. 1, pp. 316–328, 2020.

[8] J. Lopez-Sanz, C. Ocampo-Martinez, J. Alvarez-Florez, M. Moreno-Eguilaz, R. Ruiz-Mansilla, J. Kalmus, M. Gräeber, and G. Lux, "Non-linear model predictive control for thermal management in plug-in hybrid electric vehicles," *IEEE Transactions on Vehicular Technology*, vol. 66, no. 5, pp. 3632–3644, 2016.

[9] H. Min, Z. Zhang, W. Sun, Z. Min, Y. Yu, and B. Wang, "A thermal management system control strategy for electric vehicles under low-temperature driving conditions considering battery lifetime," *Applied Thermal Engineering*, vol. 181, p. 115944, 2020.

[10] C. Zhu, F. Lu, H. Zhang, J. Sun, and C. C. Mi, "A real-time battery thermal management strategy for connected and automated hybrid electric vehicles (cahevs) based on iterative dynamic programming," *IEEE Transactions on Vehicular Technology*, vol. 67, no. 9, pp. 8077–8084, 2018.

[11] S. Zhao and C. C. Mi, "A two-stage real-time optimized ev battery cooling control based on hierarchical and iterative dynamic programming and mpc," *IEEE Transactions on Intelligent Transportation Systems*, 2021.

[12] Y. Liu and J. Zhang, "Electric vehicle battery thermal and cabin climate management based on model predictive control," *Journal of Mechanical Design*, vol. 143, no. 3, 2021.

[13] J. Glos, L. Otava, and P. Václavek, "Non-linear model predictive control of cabin temperature and air quality in fully electric vehicles," *IEEE Transactions on Vehicular Technology*, vol. 70, no. 2, pp. 1216–1229, 2021.

[14] S. Zhang and W. Shen, "Rule-based control of battery external heating for electric vehicle during driving at low temperatures," *IEEE Access*, vol. 9, pp. 149 360–149 371, 2021.

[15] M. Sarmiento-Carnevali, A. Fly, and P. Piecha, "Electric vehicle cold start range estimation through battery-in-loop simulations within a virtual driving environment," 2020.

[16] N. Mancini, J. S. M. Mardall, J. Kopitz, C. R. O'donnell, D. F. Hanks, and H. Li, "Optimal source electric vehicle heat pump with extreme temperature heating capability and efficient thermal preconditioning," Apr. 6 2021, uS Patent 10,967,702.

[17] L. Feng and P. Hrnjak, "Experimental study of an air conditioning-heat pump system for electric vehicles," *SAE International Journal of Passenger Cars-Mechanical Systems*, vol. 9, no. 1, pp. 68–74, 2016.

[18] C. Liu, Y. Zhang, T. Gao, J. Shi, J. Chen, T. Wang, and L. Pan, "Performance evaluation of propane heat pump system for electric vehicle in cold climate," *International Journal of Refrigeration*, vol. 95, pp. 51–60, 2018.

[19] I. Cvok, B. Škugor, and J. Deur, "Control trajectory optimisation and optimal control of an electric vehicle hvac system for favourable efficiency and thermal comfort," *Optimization and Engineering*, vol. 22, no. 1, pp. 83–102, 2021.

[20] M. A. Fayazbakhsh and M. Bahrami, "Comprehensive modeling of vehicle air conditioning loads using heat balance method," *SAE technical paper*, vol. 2013, p. 1507, 2013.

[21] X. Lin, H. E. Perez, S. Mohan, J. B. Siegel, A. G. Stefanopoulou, Y. Ding, and M. P. Castanier, "A lumped-parameter electro-thermal model for cylindrical batteries," *Journal of Power Sources*, vol. 257, pp. 1–11, 2014.

[22] J. Chen, A. Behal, and C. Li, "Active cell balancing by model predictive control for real time range extension," in *2021 IEEE Conference on Decision and Control*, Austin, TX, USA, December 13–15, 2021.